# Cyclotron emission from quantized Hall devices: Injection of nonequilibrium electrons from contacts

Y. Kawano and Y. Hisanaga*

*Department of Basic Science, University of Tokyo, Komaba 3-8-1, Meguro-ku, Tokyo 153-8902, Japan*

S. Komiyama

*Department of Basic Science, University of Tokyo, Komaba 3-8-1, Meguro-ku, Tokyo 153-8902, Japan*
*and Japan Science and Technology Corporation (JST), Tokyo, Japan*

Emissions of cyclotron radiation associated with the inter-Landau-level transition of nonequilibrium electrons are experimentally studied in quantum-Hall-effect devices. It is confirmed that both the longitudinal resistance and the contact resistance are vanishing when the cyclotron emission (CE) is being observed. For the CE, a critical source-drain voltage $V_{SD}$ is found to exist at $V_{SD} = \hbar\omega_c/2e$, where $\hbar\omega_c$ is the inter-Landau-level energy spacing. Spatially resolved measurements reveal that the CE takes place at both of the current entry and exit corners (''hot spots'') of the Hall bars. A model of ideal current contacts is discussed. The CE on the source side is interpreted as being due to injection of nonequilibrium electrons from the source contact, and the CE on the drain side as due to an inter-Landau-level electron tunneling caused by a steep potential wall formed at the drain contact. [S0163-1829(99)04619-6]

## I. INTRODUCTION

In the quantum Hall effect (QHE) regime,[1,2] the longitudinal resistance $R_{xx}$ of a Hall-bar conductor vanishes. If the current $I$ passing through a Hall-bar conductor is infinitesimal, theories predict that the electrical power necessary to support $I$ is totally dissipated within the current contacts in the QHE regime.[3,4] In the experiments, $I$ is always finite and little is yet clarified about the mechanism of dissipation. Especially it is still unclear whether the dissipation processes take place within the contacts or in the two-dimensional electron gas (2DEG). This issue is of physical importance for it deeply relates to understanding of the kinetics of electron entry and exit at the interfaces between the 2DEG layer and the (metallic) Ohmic contacts.

By using the fountain-pressure effect of superfluid liquid helium, Klaß et al.[5] demonstrated that, in the QHE state, dissipation takes place almost totally at the diagonally opposite current entry and exit corners of the sample. The existence of these ''hot spots'' was expected earlier by Wakabayashi and Kawaji.[6] The same conclusion has been derived from the experiments of Russell et al.,[7] who applied local bolometry technique. These experiments, however, do not specify whether the dissipation takes place within the contacts or in the 2DEG.

von Klitzing et al.[8] and Zinov'ev et al.[9] reported observation of the cyclotron emission (CE) associated with the transition of electrons from higher Landau levels to lower Landau levels in GaAs/Al$_x$Ga$_{1-x}$As Hall-bar devices. These CE experiments demonstrated the presence of nonequilibrium electrons among Landau levels, and indicated that power is dissipated at least partly in the 2DEG. A similar conclusion has been derived recently by Roshko, Dietsche, and Challis,[10] who found the emission of phonons with the cyclotron energy $\hbar\omega_c$ in Si metal-oxide-semiconductor field-

effect transistors (MOSFETs). Unfortunately, however, the CE experiments were carried out at large currents where the QHE breaks down to yield a finite longitudinal resistance $R_{xx}$.[8,9] Also in the phonon experiments,[10] $R_{xx}$ is finite at relatively low magnetic fields where the inter-Landau-level transition of the 2DEG is demonstrated: Although phonons are detected in the condition of $R_{xx}=0$ in higher magnetic fields, those phonons cannot be unambiguously ascribed to those from the 2DEG without interpretation.

Despite these preceding works, our present understanding is thus not satisfactory. First, we still do not have direct evidence of dissipation in the 2DEG in the unambiguous condition that both $R_{xx}$ and the excess contact resistance $R_C$ are vanishing. Secondly, it is completely unclear whether the dissipation in the 2DEG, if any, occurs in the source-side corner (where electrons enter the 2DEG) or in the drain-side corner (where electrons leave the 2DEG), or in both. Finally, if dissipation indeed takes place in the 2DEG with $R_{xx}+R_C=0$, its physical mechanism should be clarified: The coexistence of dissipation in the 2DEG and the vanishing of $R_{xx}+R_C$ may not be a trivial issue. Based on a simple theoretical model, van Son and co-workers suggested that local nonequilibrium distribution of electrons should be totally absent, yielding no dissipation in the 2DEG if the source-drain voltage $V_{SD}$ is smaller than $\hbar\omega_c/2e$ but nonequilibrium electrons come to be injected from the source contact when $V_{SD}$ exceeds $\hbar\omega_c/2e$.[11,12] In this model, nonequilibrium electron distribution and resultant dissipation in the 2DEG are expected only in the source-side (electron entry) corner. All the measurements in the above[5,7–10] are carried out with $V_{SD}$ far larger than $\hbar\omega_c/2e$, and comparison with theory is impossible.

In this work we study CE, which serves as a powerful tool to probe exclusively the local nonequilibrium electron distribution in the 2DEG. The purpose of this work is (i) to gain

unambiguous experimental proof of local nonequilibrium distribution of electrons in the 2DEG under the condition $R_{xx}+R_C=0$, (ii) to extend the study toward smaller $V_{SD}$ values in order to make comparison with theory possible, and (iii) to specify the location(s) of the nonequilibrium distribution. The final goal of this work is to derive a consistent picture of the kinetics of electron entry and exit in QHE Hall bars at finite currents based upon these experimental results.

This paper is organized as follows. After a brief introduction of experimental methods in Sec. II, experimental results are presented in Sec. III. In Sec. III A we study the QHE state for the filling factor of $\nu=2$ and show that CE is observed (and thus finite dissipation occurs in the 2DEG) under the condition $R_{xx}+R_C=0$. In Sec. III B, we study dependence of the CE intensity on $V_{SD}$ and find that the CE rapidly weakens and practically vanishes for $V_{SD}<\hbar\omega_c/2e$. Dissipation in the 2DEG is thus suggested to occur only when $V_{SD}$ exceeds $\hbar\omega_c/2e$. Section III C describes spatially resolved measurements and shows that the CE occurs at both of the electron entry and exit corners. This suggests that dissipations of comparable amplitudes take place on the 2DEG side at both of these corners. At the beginning of Sec. IV, it is argued that an electron heating model due to QHE breakdown at the current entry and exit corners is inappropriate to interpret the experimental findings. The model of van Son *et al.* of current contacts is also suggested to be not completely satisfactory for the interpretation. To derive a consistent picture, Sec. IV A is devoted to construction of a theoretical model that deals with electron kinetics both inside a QHE Hall-bar conductor and at the interface to metallic contacts. In Sec. IV B the generation of nonequilibrium distribution in the 2DEG for $V_{SD}>\hbar\omega_c/2e$ is derived in a natural way and explained as a general property of ideal QHE conductors with current contacts. Experimental results are reasonably interpreted in terms of the proposed model, giving a consistent picture of dissipation in QHE Hall bars. Section V summarizes important conclusions.

## II. EXPERIMENTAL METHODS

Samples of three different geometries, labeled as $E1-E3$ in Fig. 1, are used in the present work. The samples are fabricated on a GaAs/Al$_x$Ga$_{1-x}$As heterostructure crystal with the 4.2-K mobility of $80\,\text{m}^2/\text{V s}$ and the 4.2-K electron density of $2.6\times10^{15}/\text{m}^2$. Figure 1(a) shows a long 2DEG Hall bar (sample $E1$) of a channel width of 200 $\mu$m and a total length of 53 mm. The 2DEG channel runs zigzag in a square of $4\times4\,\text{mm}^2$. An equivalent geometry is illustrated in the right panel of Fig. 1(a). Figure 1(b) shows a Hall-bar array (sample $E2$), in which 197 parallel Hall bars are jointed in series 67 times. Each Hall bar is 40 $\mu$m long and 20 $\mu$m wide. Figure 1(c) shows a standard Hall bar of 3 mm length and 1.5 mm width (sample $E3$), which is used for the study of spatial distribution of the cyclotron emission.

Highly sensitive photoconductive detectors based on the cyclotron resonance of high-mobility 2DEG systems in GaAs/Al$_x$Ga$_{1-x}$As heterostructures are used.[13,14] The detectors are fabricated on the same GaAs/Al$_x$Ga$_{1-x}$As heterostructure crystal as that for samples $E1-E3$. The spectral response of the detectors has been studied by using a Fourier transform spectrometer, and shown to be due to sharp cyclo-
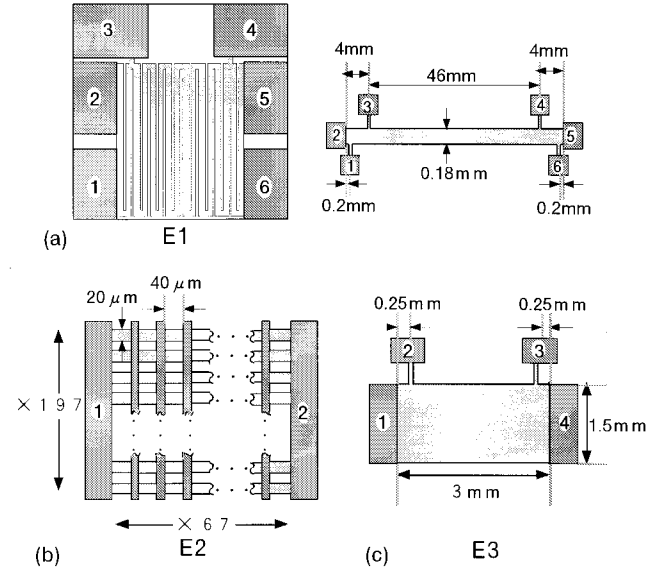


FIG. 1. Schematic of the samples used. (a) Sample $E1$: a long 2DEG Hall bar. An equivalent geometry is illustrated in the right panel. (b) Sample $E2$: an array of $67\times197$ Hall bars. (c) Sample $E3$: a standard Hall bar.

tron resonance of the 2DEG with the full width at half maximum of about $2.5\,\text{cm}^{-1}$ in the range of magnetic fields studied. The absolute relationship between the detected wavelengths and the applied magnetic fields is determined through the Fourier transform spectroscopy.

The sample and the detector are, respectively, placed at the centers of two superconducting solenoids installed in a liquid helium cryostat. Radiation from the sample is guided through a 29-cm-long metal light pipe to the detector. Samples are excited with an ac current at a frequency of 20 Hz and the detector signals are studied by using a lock-in amplifier. All the measurements are carried out at 4.2 K.

Below, we will denote, by $R_{ij,kl}$, the multiterminal resistance obtained by passing current from contact $i$ to contact $j$ and measuring the voltage between contact $k$ and contact $l$.

## III. EXPERIMENTAL RESULTS

The two-terminal resistance $R_{2t}$ of a Hall-bar device may be simply approximated by the sum of the longitudinal resistance over the full length of the Hall bar, $R_{xx}$, the source/drain excess contact resistances, $R_{SC}$ and $R_{DC}$,[4] and the Hall resistance, $R_H$:

$$R_{2t}=R_{xx}+R_{SC}+R_{DC}+R_H. \tag{3.1}$$

When current $I$ is passed through the device, the total power input is given by $R_{2t}I^2=(R_{xx}+R_{SC}+R_{DC}+R_H)I^2$. The term $(R_{xx}+R_{SC}+R_{DC})I^2$ leads to generation of nonequilibrium electron distribution and causes dissipation in the interior region of the 2DEG layer. The CE can be accordingly expected from this term. The present experiments primarily deal with the Hall resistance term $R_HI^2$ that does not cause dissipation in the interior region. The power, $P_H=R_HI^2$, has been suggested to be totally dissipated at the electron entry ($P_S$) and exit ($P_D$) corners forming ''hot spots'' in the Hall bar;[5-7] viz.,

$$P_H = P_S + P_D.$$

From the general point of view, these dissipations may occur, respectively, partly on the contact side ($P_{S(D)-C}$) and partly on the 2DEG side ($P_{S(D)-2DEG}$) of these corners; viz.,

$$P_S = P_{S-C} + P_{S-2DEG},$$

$$P_D = P_{D-C} + P_{D-2DEG}.$$

Experimentally, however, the occurrence of dissipation on the 2DEG side, $P_{S-2DEG}$ and/or $P_{D-2DEG}$, has not been proved in an unambiguous manner because a possible contribution from the term $(R_{xx} + R_{SC} + R_{DC})I^2$ was not ruled out completely in the existing experiments. Dissipation processes may be dominated by phonon emissions in any component mentioned in the above. However, the components $P_{S-2DEG}$ and $P_{D-2DEG}$ can be exclusively probed by the CE when investigated under the condition $R_{xx} + R_{SC} + R_{DC} = 0$.

### A. Cyclotron emission in the dissipationless QHE state

Figure 2(a) displays the two-terminal resistance $R_{25,25}$ of sample $E1$ and shows that $R_{xx}$ vanishes in the QHE states of $\nu = 2$ ($B = 5.65$ T) and $\nu = 4$ ($B = 2.8$ T) but largely exceeds the Hall resistance outside the QHE states. We study CE from this sample in the vicinity of the QHE state of $\nu = 2$. The magnetic field for the detector is fixed at $B_D = 5.90$ T, where the detector exhibits sharp spectral response at the frequency of $79.9$ cm$^{-1}$. The current for the sample is $I = 50 \mu$A. As the magnetic field $B$ is scanned, a sharp emission line shows up at around $B = 5.85$ T, as displayed by the thick solid line in the top panel of Fig. 2(b), where the two-terminal resistance $R_{2t} = R_{25,25}$ is shown together. The emission band is located at a magnetic field position slightly higher than the $\nu = 2$ QHE plateau. To study CE exactly in the $\nu = 2$ QHE state, we increase the electron density $n_s$ of the sample by illumination of an infrared light-emitting diode (LED). At each time of a slight increase in $n_s$, we carry out similar measurements. The experimental data shown in the middle and bottom panels of Fig. 2(b) are examples taken from such series of measurements.

The observed line shape of the photoresponse signals, $V_{sig}$, is strongly affected by the sharp minimum of the total dissipation ($R_{2t}I^2$) at $\nu = 2$. To obtain the correct shape of the emission spectra, $V_{sig}$ is normalized as $V_{sig}/R_{2t}I^2$ and displayed in the corresponding columns in Fig. 2(c). The numbers marked on the vertical scales of Fig. 2(c) make it possible to compare the relative intensity among the three emission lines.

In the panels at the top and bottom of Fig. 2(c), the peak position of the emission line corresponds to $\nu = 1.94$ and $\nu = 2.07$, respectively, where the longitudinal resistances $R_{xx}$ (48 k$\Omega$ and 18 k$\Omega$, respectively) are substantially larger than the Hall resistance. Therefore, the cyclotron emissions there are ascribed primarily to the (conventional) hot electron effects arising from the $R_{xx}I^2$ term. The situation is different in the middle panel, where the emission peak is located exactly at $\nu = 2.00$, where $R_{2t}$ is seen to be equal to the quantized Hall resistance $R_H = (h/e^2)(1/2) = 12.9$ k$\Omega$.

In order to confirm the correct quantization of $R_{2t}$ more rigorously, we replot these data together with the three-
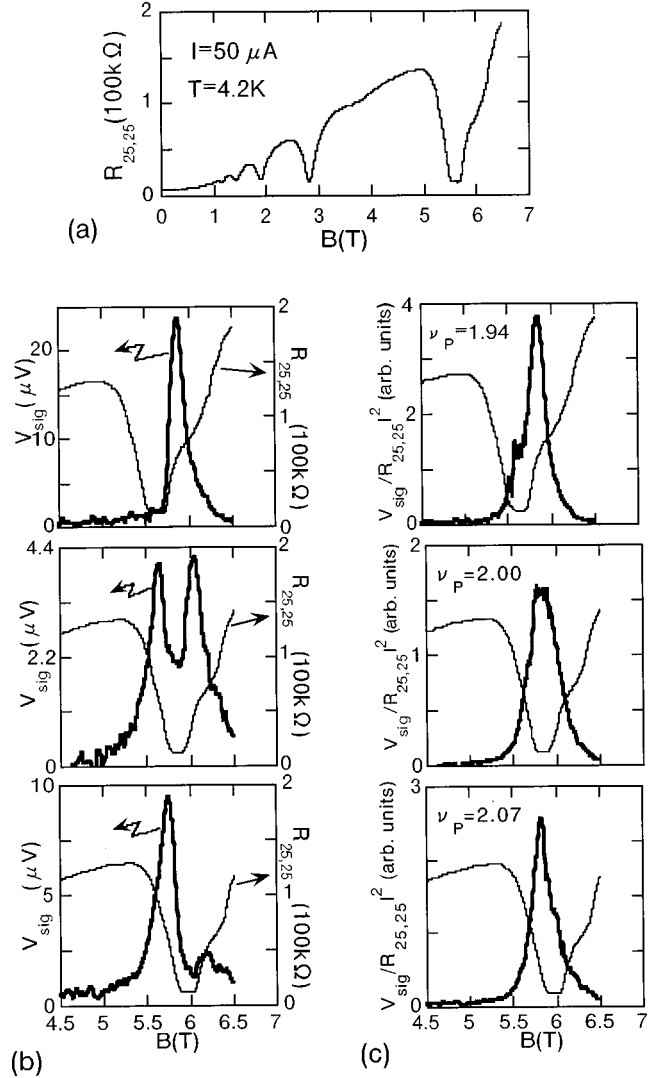


FIG. 2. (a) The two-terminal resistances, $R_{2t} = R_{25,25}$, vs $B$ in sample $E1$. (b) Cyclotron emissions (thick solid lines) $V_{sig}$ and $R_{2t}$ (thin solid line) as a function of $B$ applied to the sample. The electron density increases slightly from the top to the bottom. (c) The emission intensity normalized by the total power dissipation (thick solid lines), $V_{sig}/R_{2t}I_2$, and $R_{2t}$ (thin solid lines) as a function of $B$.

terminal resistances $R_{25,24}$, and $R_{25,65}$, along with the two-terminal resistance $R_{2t} = R_{25,25}$ in Fig. 3. We see that both $R_{25,24}$ and $R_{25,65}$ are vanishing in a finite magnetic-field range around $\nu = 2.00$ ($B = 5.85$ T), where $V_{sig}$ values are maximal. Since the sum $R_{25,24} + R_{25,65}$ includes both of the excess contact resistances, $R_{SC}$ and $R_{DC}$, and $R_{xx}$ over a nearly full length of the 2DEG channel, the simultaneous vanishing of $R_{25,24}$ and $R_{25,65}$ assures that $R_{xx} + R_{SC} + R_{DC}$ are vanishing. Measurements with higher sensitivity showed that $R_{25,24} + R_{25,65} \sim 0.08$ k$\Omega = 6 \times 10^{-3} R_H$ at $\nu = 2.00$. We thus conclude that nonequilibrium electron distribution is produced in the 2DEG under the condition where $R_{xx} + R_{SC} + R_{DC}$ is negligibly small compared to $R_H$. This also implies that the dissipation, $P_{S(D)-2DEG}$, in the 2DEG is finite under this condition.

The radiation power reaching the detector is on the order of 0.1 pW at $\nu = 2.00$, which, together with the consideration
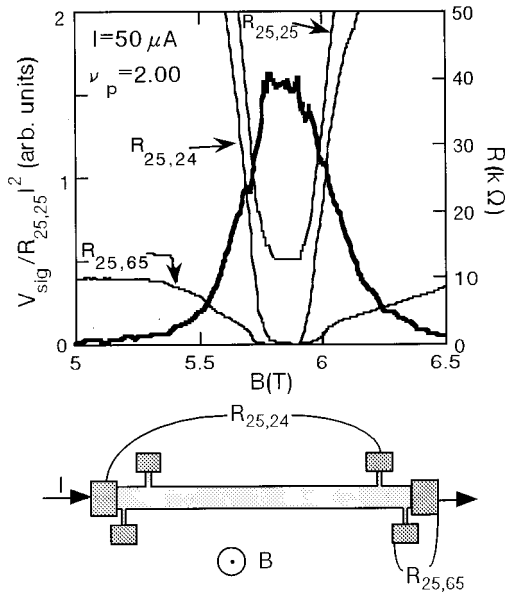
FIG. 3. The normalized emission intensity (thick solid line), $V_{sig}/R_{2t}I_2$, compared with $R_{2t}$ (thin solid line) and the three-terminal resistances $R_{25,24}$ and $R_{25,65}$ (thin solid lines) as a function of $B$. The condition is the same ($\nu_p=2.00$) as that for the middle panel of Fig. 2(b).

of present optics, suggest that the power dissipated via cyclotron radiation comprises on the order of $10^{-6}$ of the total dissipation $P_H=P_S+P_D=R_HI^2$. Returning to Fig. 2(c), we note that the amplitude of $V_{sig}/R_{2t}I^2$ in the QHE state ($\nu=2.00$) is somewhat smaller than but comparable to those in the adjacent non-QHE states ($\nu=1.94$ and $\nu=2.07$). This implies that the efficiency of energy conversion to the CE from the $R_HI^2$ term is smaller than but comparable to that from the $R_{xx}I^2$ term: An analysis shows that the efficiency differs only by a factor of about 3.

We also note that the $B$ position at which $V_{sig}/R_{2t}I^2$ takes a maximum is the same among the three lines in Fig. 2(c), being at $B_p=(5.85\pm0.06)$ T. The associated cyclotron effective mass is derived to be $m_c^*=(0.069\pm0.0007)m_0$ with the free electron mass $m_0$. This mass value is in substantial agreement with the bulk cyclotron effective mass in a 2DEG with $\nu_s=3.0\times10^{11}/cm^2$ at $B\sim6$ T.[15]

### B. Threshold current for the cyclotron emission

The current, $I=50\,\mu A$, applied in the measurements for Figs. 2 and 3, corresponds to $V_{SD}=R_HI=660$ mV that is by a factor of 66 larger than $\hbar\omega_c/e=10$ mV. The CE is visible down to $I\sim10\,\mu A$, below which the measurements become difficult due to the poor signal-to-noise ratio. To carry out lower-current measurements, we study sample $E2$, where the total current $I_{total}$ through the sample is divided by 197 Hall bars arranged in parallel. The current passing through each Hall bar is thus $I_{each}=I_{total}/197$. The two-terminal resistance $R_{2t}=R_{12,12}$ of sample $E2$ is depicted as a function of $B$ in the inset of Fig. 4(a). The center of the $\nu=2$ QHE state is located at $B=5.7$ T, where $R_{12,12}=4$ k$\Omega$ is close to the expected quantized value $(67/197)R_H=4.39$ k$\Omega$ with $R_H=(h/e^2)(1/2)$. We accordingly suggest that $R_H$ dominates at $\nu=2.0$.
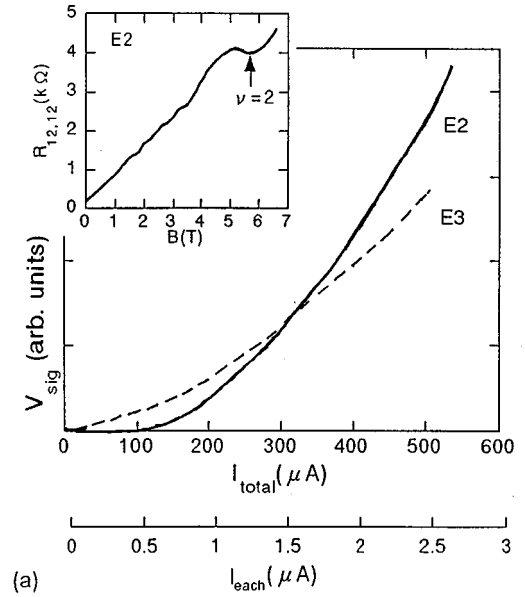


(a)
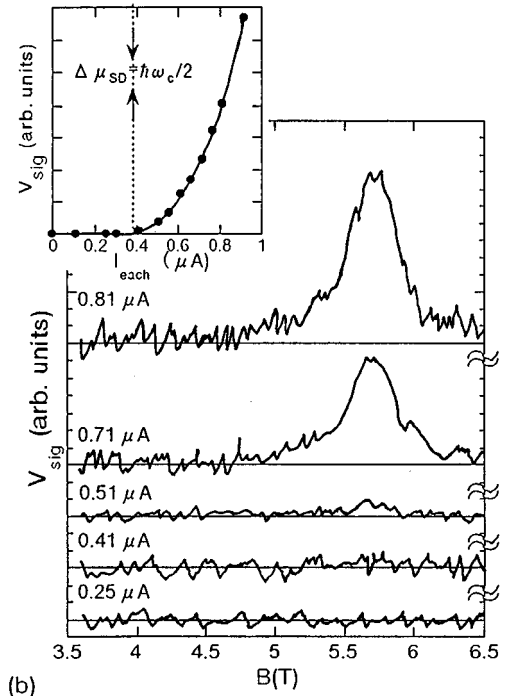


(b)

FIG. 4. (a) Dependence of the emission-peak intensity on the current in sample $E2$ (the solid line) and sample $E3$ (the broken line). The scale of $I_{each}$ shows the current for each Hall bar in sample $E2$. The inset shows $R_{2t}$ vs $B$ in sample $E2$. (b) The emission spectra in the sweep of $B$ in sample $E2$ at different current levels. The inset shows $I_{each}$ dependence of the emission-peak intensity.

The cyclotron emission is studied at $\nu=2.00$ ($B=5.70$ T) by applying $B_D=5.65$ T to the detector. The solid line in Fig. 4(a) shows the emission intensity as a function of current where the current is applied in square waves alternating between zero and given values. For the sake of comparison with the data of a single Hall bar, the CE intensity in sample $E3$ at $\nu=2.0$ is shown together. We note that the line shapes of the two curves are substantially different from each
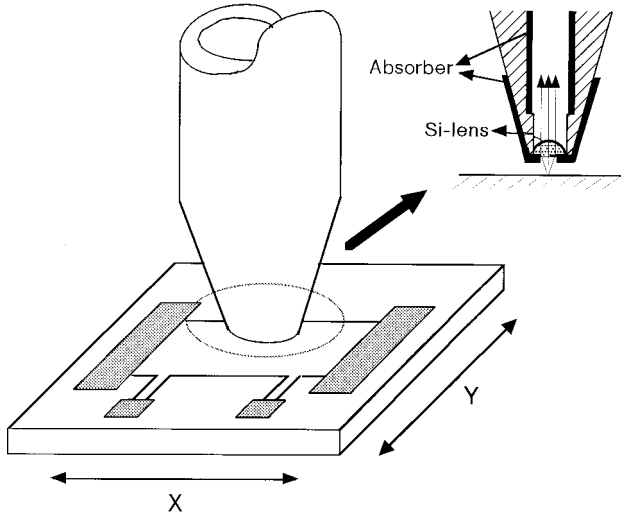
FIG. 5. Schematic representation of the arrangements for studying the spatial distribution of cyclotron emission. The radiation emitted from sample $E3$ is collimated by a Si lens and guided to the detector. The sample is placed on an $X$-$Y$ translation stage. See the text for detail.

other. Namely, $V_{\text{sig}}$ in sample $E2$ decreases steeply with decreasing $I_{\text{total}}$ below 200 $\mu$A, and practically vanishes below 100 $\mu$A. This anomalous feature is not seen in $E3$, which consists of a single Hall bar.

Figure 4(b) displays emission spectra in sample $E2$ at several values of $I_{\text{each}}$ below 1 $\mu$A. The intensity of CE rapidly decreases as $I_{\text{each}}$ decreases from 0.81 $\mu$A to 0.51 $\mu$A, below which the CE is no longer discernible. The inset of Fig. 4(b) elucidates the dependence of the emission-peak intensity on the current in the range below $I_{\text{each}}=0.9\,\mu$A. The result strongly suggests the vanishing of CE below a current about $I_{\text{each}}=0.4\,\mu$A. This critical current corresponds to $V_{\text{SD}}=\hbar\omega_c/2e=5$ mV or $\Delta\mu_{\text{SD}}=\hbar\omega_c/2$, where $\Delta\mu_{\text{SD}}$ is the electrochemical potential difference between the source and drain contacts. This suggests that local nonequilibrium distribution vanishes in the 2DEG for $\Delta\mu_{\text{SD}}<\hbar\omega_c/2$, implying that $P_{S-2\text{DEG}}+P_{D-2\text{DEG}}$ is zero for $\Delta\mu_{\text{SD}}<\hbar\omega_c/2$ but becomes finite for $\Delta\mu_{\text{SD}}>\hbar\omega_c/2$.

### C. Spatial distribution of the cyclotron emission

To specify the location of the CE, we apply the experimental setup illustrated in Fig. 5. Sample $E3$ is mounted on a mechanical $X$-$Y$ translation stage movable from the outside of the cryostat. The radiation from the movable sample is collimated by a convex lens attached at the end of a fixed light pipe with a 1-mm $\phi$ aperture. The radiation is guided to a detector placed at the other end of the light pipe. The lens, made of pure silicone crystal, is of a 1.2 mm focal length. The obtained spatial resolution is about 300 $\mu$m.

Figure 6(a) displays the two-terminal resistance $R_{2t}=R_{14,14}$ and the three-terminal resistance $R_{3t}=R_{14,23}$ against $B$ in sample $E3$ at $I=73\,\mu$A, and shows the vanishing of $R_{3t}$ and the quntization of $R_{2t}=(h/e^2)(1/2)$ at $\nu=2$ ($B=6.15$ T). The measurement of CE is carried out at $\nu=2$ ($B=6.15$ T) with $I=73\,\mu$A, where $B_D$ is adjusted to 6.10 T.
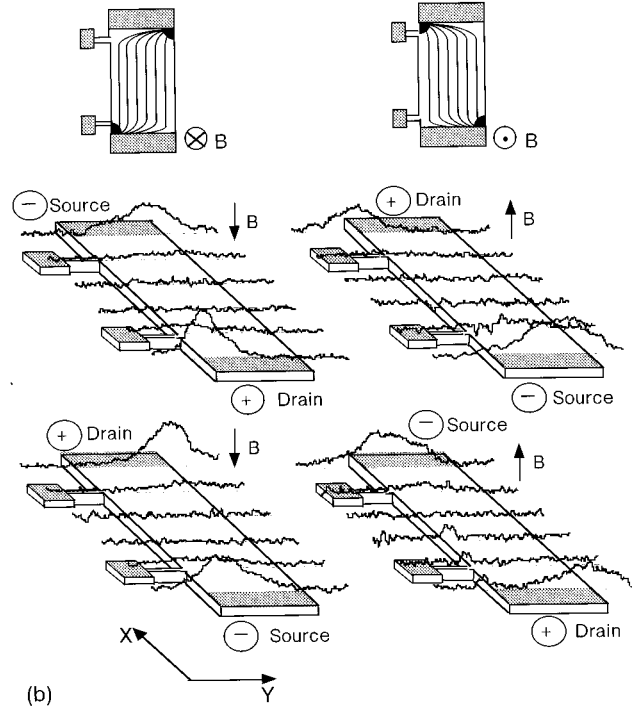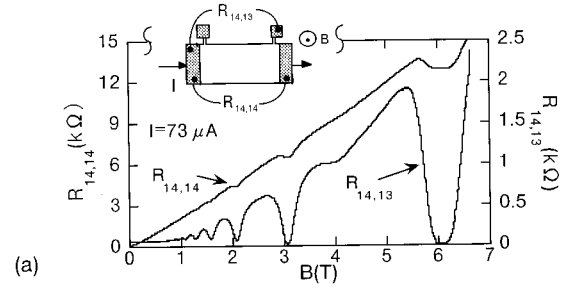


FIG. 6. (a) The two-terminal resistance $R_{2t}=R_{14,14}$ and three-terminal resistance $R_{3t}=R_{14,13}$ as a function of magnetic field at $I=73\,\mu$A in sample $E3$. (b) Spatial distribution of the cyclotron emission at $I=73\,\mu$A in sample $E3$ for the four configurations of the polarity of $B$ and $I$. Illustrations at the top show classical equipotential lines in a QHE device.

Figure 6(b) shows the spatial distribution of the CE intensity for four different configurations of the polarities of $B$ and $I$, where the scan is made along the widthwise direction ($Y$) of the sample while the lengthwise position ($X$) is shifted at a step of 600 $\mu$m for each scan. Classical equipotential lines along with the current entry and exit corners are schematically shown in the top panel of Fig. 6(b). In each configuration of $B$ and $I$, the CE is seen at both the current entry and exit corners. The fact that the locations change to the other two diagonally opposite corners upon reversal of the magnetic-field polarity assures that the observed profile of the CE is substantially independent of inhomogeneities of the Hall-bar sample and is of intrinsic nature. Our experiments thus demonstrate that the local nonequilibrium distribution is produced on the 2DEG side at both of the corners. Noting that the CE intensity is comparable between the two corners, $P_{S-2\text{DEG}}\sim P_{D-2\text{DEG}}$ is also suggested at $I=73\,\mu$A. The cyclotron effective masses were confirmed to be substantially equal to each other between the two corners.

## IV. DISCUSSION

We summarize our experimental results as follows. (i) CE occurs in the condition where $R_{xx}+R_C+R_D \approx 0$: This was directly confirmed for $10\,\mu\text{A} \lesssim I < 80\,\mu\text{A}$, and is strongly suggested to apply also to the lower-$I$ range. (ii) The CE is visible until $I$ is reduced to about 0.4 $\mu$A ($\Delta\mu_{SD}=\hbar\omega_c/2$), below which the CE is no longer discernible. This strongly suggests that dissipation in the 2DEG, $P_{S-2\text{DEG}}+P_{D-2\text{DEG}}$, is absent for $\Delta\mu_{SD}<\hbar\omega_c/2$ but sets in at $\Delta\mu_{SD}=\hbar\omega_c/2$. (iii) At $I=73\,\mu$A, CE occurs in both of the current entry and exit corners. (We defer discussion of the cyclotron effective mass to Sec. IV C.) Although these conclusions are derived from samples of different geometry, we do not see a reason to suppose them to be geometry specific, and assume that they are intrinsic properties of Hall-bar conductors in the QHE state.

The occurrence of CE in the vicinities of the current entry and exit corners indicates that a significant population of electrons (holes) is created there in the upper (lower) Landau level. This local nonequilibrium electron distribution may be most simply characterized by an effective electron temperature $T_e$ that is higher than the lattice temperature $T_L$. Noting the observed CE intensity together with the cyclotron energy $\hbar\omega_c=10$ meV, we roughly estimate $\Delta T_e \equiv T_e-T_L$ to be about 10 K at $I=50$–73 $\mu$A.

Let us consider how electrons can be locally heated at the corners of a Hall bar. Existing experiments indicate that nearly all power, $P_H=P_H I^2$, is dissipated at the corners.[5,7] Therefore, no matter how and in which mechanism the power is dissipated it must eventually work to locally heat up the lattice and electron systems in the vicinity of these corners (hot spots), both on the contact and 2DEG sides. The overall temperature rise at the hot spots, however, is estimated in Klaß et al.'s experiments to be as small as $\Delta T=10\,\mu$K at $I=30\,\mu$A ($\nu=2$),[5] which may be far too small to account for the observed CE. Accordingly we need to consider a specific mechanism for heating up of the 2DEG. There are two possible mechanisms as discussed below.

The first mechanism is related to strong electric fields at the corners.[6] Several authors[5,10] suggest that the strong electric fields cause the QHE to break down,[16,17] yielding hot electrons at the corners. However, experiments on the QHE breakdown indicate that, in order for electrons to be appreciably heated, strong electric fields have to be distributed over macroscopic length scales because the process of heating occurs as an avalanche multiplication of electron-hole pairs.[18,19] The critical electric field $E_C$ and the necessary length scale $L_B$ are shown to be about $E_C=20$ kV/m and $L_B \sim 100\,\mu$m at $B=6$ T ($\nu=2$) for the 2DEG in the same crystal as the one used in this work.[18,19] It follows that the lowest $V_{SD}$ value at which the QHE-breakdown-induced heating is expected to take place is $E_c L_B/2=1$ V $\sim 100\hbar\omega_c/e$ ($I \sim 80\,\mu$A), which is far larger than the observed critical value $V_{SD}=\hbar\omega_c/2e$ ($I=0.4\,\mu$A) for the CE. Furthermore, if the QHE breakdown were relevant, we expect that the CE in the source-side (electron entry) corner should dominate because the heated electrons at the drain-side (electron exit) corner are rapidly absorbed by the drain contact and will not effectively contribute to the CE. This is not consistent with our observation and suggests that the

breakdown-induced heating is not a dominant mechanism at $I=73\,\mu$A [Fig. 6(b)]. (We do not rule out the possibility that this mechanism is important for $I>80\,\mu$A, which is beyond the scope of this work.) The strong electric fields at the corners of Hall bars may also induce Zener-type tunneling transition of electrons to higher Landau levels.[20,21] This effect is related to the second mechanism described below.

The second mechanism, which we suppose to be relevant to our experimental results, is directly related to the kinetics of electron entry (exit) to (from) the 2DEG. van Son and co-workers argued that nonequilibrium electrons are injected from the source contact when $\Delta\mu_{SD}$ exceeds $\hbar\omega_c/2$; viz., $P_{S-2\text{DEG}}>0$. Although this prediction is in accordance with a part of our results, these authors do not expect the occurrence of nonequilibrium distribution at the drain-side corner; viz., $P_{D-2\text{DEG}}=0$. They suggested also that $R_{xx}+R_{SC}$ becomes finite coincidentally with the occurrence of $P_{S-2\text{DEG}}$. These two do not agree with our findings. To derive a consistent picture, we devote the following two subsections to rather comprehensive theoretical discussions of a model of a QHE Hall-bar conductor at finite currents. The occurrence of nonequilibrium electron distribution on the 2DEG side at both of the corners will be naturally derived from the model. We will show that all of our experimental findings are consistently interpreted in terms of our model.

### A. Model of current contacts

Injection of nonequilibrium electrons from a source contact was suggested qualitatively by Yoshihiro et al.[22] A model of current contact was discussed in a more quantitative way by van Son and co-workers,[11,12] who extended Büttiker's model of contacts.[3,4] In the following we will elaborate the model of QHE Hall-bar conductors at finite currents following the original arguments of van Son and co-workers.

Let us begin with $I=0$. Figure 7(a) schematically shows a profile of the electrostatic potential energy $U_0(r)$ for a 2DEG sample including two current contacts when it is in the equilibrium state with $I=0$. The 2DEG channel is characterized by a flat interior region bounded by potential walls at both sides. The current contacts are supposed to be metallic, in which the Fermi energy and the density of states are far larger than those in the 2DEG. The regions of contacts are characterized by deep potential wells. The contacts are ideal Ohmic ones, and there is no Schottky-type barrier between the 2DEG and the contacts. (Random potentials in the contacts are ignored for simplicity.) All the electron states are completely filled with electrons up to the Fermi level $\varepsilon_F$. The electrons in the 2DEG layer move along equipotentials, $U_0(r)=$const, with a drift velocity proportional to the slope of a Landau level, and edge states are formed along the potential walls. In the quantum Hall regime with the indicated polarity of magnetic field, electrons move from the left to the right along the upper edge states. As depicted in Fig. 8(a), electrons with the energies of $\varepsilon_F-\hbar\omega_c/2<\varepsilon<\varepsilon_F$ move along the upper edge states and enter the right-hand-side contact. The electrons that have entered the contact yield (dissipationless) magnetization current within the contact

(a)



(b)



(c)
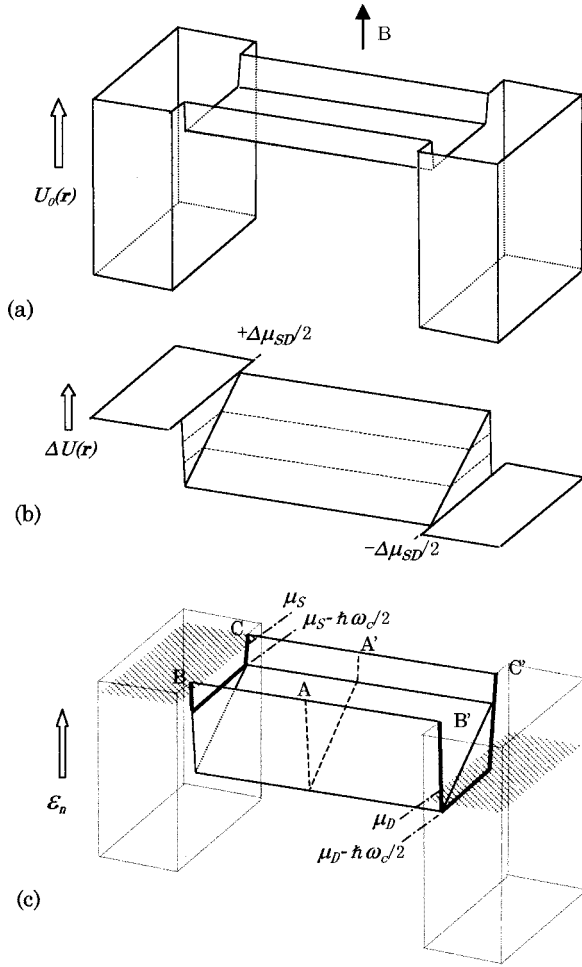
FIG. 7. (a) Schematic perspective view of the electrostatic potential energy $U_0(r)$ for a 2DEG sample with current contacts when the net current is zero. (b) Schematic perspective view of the change in the electrostatic potential $\Delta U(r)$ induced when the net current $I = \nu(e/h)\Delta\mu_{SD}$ is passed through the sample. (c) Schematic perspective view of the highest occupied Landau level in the presence of the net current. The boundaries between the contacts and the 2DEG are indicated by the bold lines.



FIG. 8. Electron trajectories in the highest occupied Landau level, under three conditions, (a) $\Delta\mu_{SD}=0$, (b) $0<\Delta\mu_{SD}<\hbar\omega_c/2$, and (c) $\hbar\omega_c/2<\Delta\mu_{SD}$. Schematic representations of Landau levels on the cross section $A$-$A'$ in Fig. 7(c) are displayed in the left column.

and transferred to the lower corner of the contact, from which electrons leave the contact through the lower edge states. The kinetics of electrons is equivalent in the left-hand-side current contact, and the global magnetization current circulates around the entire region of the sample.

When $I \neq 0$, $\mu_S$ and $\mu_D$ differ from $\varepsilon_F$, respectively, as $\mu_s = \varepsilon_F + \Delta\mu_{SD}/2$ and $\mu_D = \varepsilon_F - \Delta\mu_{SD}/2$. The contacts feed all the outgoing states with electrons up to their respective electrochemical potentials, and absorb all the incident electrons.[3] The upper edge states and the lower edge states are, respectively, characterized by the electrochemical potentials of $\mu_S$ and $\mu_D$. The electrostatic potential $U_0(r)$ will be accordingly modified due to the development of Hall polarization fields. Let $U(r)$ be the modified potential. The change in the electrostatic potential, $\Delta U(r)=U(r) - U_0(r)$, can be assumed to be equal to the change in the electrochemical potential, $\Delta\mu_{(r)}$, inside the contacts and along the edge states, because the density of states there is sufficiently large.[23] We therefore take $\Delta U(r)=+\Delta\mu_{SD}/2$

for the source contact (with $\mu_S$) and the upper edge states, and take $\Delta U(r) = -\Delta\mu_{SD}/2$ for the drain contact (with $\mu_D$) and the lower edge states. The zero screening length is assumed in the contact and a finite one is assumed in the 2DEG. The perspective view of the resulting $Y(r)$ is schematically shown in Fig. 7(b), where the slope of the Hall potential is assumed to be a constant for simplicity. This profile is similar to that suggested by Kawaji.[24] The exact shape of $\Delta U(r)$ inside the 2DEG is not important for the discussion.

The true trajectory of electrons is given by the equipotential lines of $U(r)=U_0(r)+\Delta U(r)$, which are not equal to the classical Hall current trajectories formed along the contour lines of $\Delta U(r)$.[25] We should note that due to the difference, $\Delta\mu_{SD}=\mu_S - \mu_D > 0$, a "potential barrier" develops in the junction region to the source contact and a "potential fall" is formed in the junction region to the drain contact. Landau levels are formed approximately as $\varepsilon_n(r)=(n+1/2)\hbar\omega_c+U(r)$ in the 2DEG. We give in Fig. 7(c) a schematic perspective view of the highest occupied Landau level. The boundaries between the contacts and the 2DEG are indicated by the heavy solid lines in Fig. 7(c). Deep inside the conductor away from both of the contacts, say, on the cross section of $A$-$A'$ in Fig. 7(c), the Landau level will be filled with electrons up to $\mu_S$ and $\mu_D$, respectively, at the opposite edges as schematically shown in the left column of Figs. 8(b) and 8(c). Let us consider how trajectories along the equipo-

tentials are fed by the contacts by noting the profile of the Landau level shown in Fig. 7(c). Since all the trajectories below $\varepsilon = \mu_D$ are completely occupied, it suffices to consider only the trajectories with $\varepsilon > \mu_D$ for considering the nonequilibrium distribution. We thus pay attention to the "Fermi-surface current" [25] below.

When $\Delta\mu_{SD}$ is smaller than $\hbar\omega_c/2$, the relevant trajectories ($\mu_D < \varepsilon < \mu_S$) form edge states as shown in Fig. 8(b).[26] The upper edge states along the cross section $C$-$C'$ in Fig. 7(c) are completely fed by the source contact while the lower edge states along cross section $B$-$B'$ in Fig. 7(c) are empty. The electrons that move along the upper edge states are absorbed by the drain contact and release their excess energies within the drain contact. Holes are created inside the source contact at the lower corner and release their excess energies within the source contact. Dissipation accordingly takes place equally at these diagonally opposite corners within the contacts.[4] Thus, no local nonequilibrium distribution of electrons is produced in the 2DEG and *dissipation occurs totally within the contacts*; viz, $P_S = P_D$ and $P_{S-2\text{DEG}} + P_{D-2\text{DEG}} = 0$ when $\Delta\mu_{SD} < \hbar\omega_c/2$.

When $\Delta\mu_{SD}$ exceeds $\hbar\omega_c/2$, the relevant electron trajectories ($\mu_D < \varepsilon < \mu_S$) are divided into two groups. The first group is of energies $\varepsilon > \mu_S - \hbar\omega_c/2$ and consist of only edge states. The kinetics of electrons in these edge states are similar to those in the case of $\Delta\mu_{SD} < \hbar\omega_c/2$ as shown in the upper panel of Fig. 8(c), yielding dissipation only within the contacts. The second group of trajectories is of energies $\mu_D < \varepsilon < \mu_S - \hbar\omega_c/2$ and consists of the lower edge states, the states in the interior region, and the states along the potential barrier and fall, as schematically shown in the lower panel of Fig. 8(c). The lower edge states are empty because $\varepsilon > \mu_D$. It is of decisive importance that the potential barrier prevents the source contact from directly feeding these trajectories as originally pointed out by van Son and co-workers.[11,12] It follows that *electrons can be injected from the source contact only through tunneling*. The electrons injected through tunneling in the vicinity of this corner move along the potential barrier, and travel toward the right following the trajectories in the interior region. The electrons that have reached the potential fall *move along the potential fall* until they are finally absorbed by the drain contact at the upper corner.

The electrons with energies $\mu_D < \varepsilon < \mu_S - \hbar\omega_c/2$ thus enter the 2DEG layer at the lower left corner and leave the 2DEG layer at the upper right corner. From the kinetics of electrons discussed in the above for $\mu_{SD} > \hbar\omega_c/2$ we can expect nonequilibrium electron distribution to occur on the 2DEG side of both corners as discussed in the next subsection.

### B. Generation of nonequilibrium electron distribution

Under the condition $\Delta\mu_{SD} < \hbar\omega_c/2$, no dissipation takes place in the 2DEG as discussed in the above. This accounts for the absence of CE for $\Delta\mu_{SD} < \hbar\omega_c/2$ in the present experiments.

Under the condition $\Delta\mu_{SD} > \hbar\omega_c/2$ the electron trajectories with $\mu_D < \varepsilon < \mu_S$ include states in the interior region. The entry (exit) of electrons into (out of) these bulk states can be affected by the potential barrier (fall) in such a way
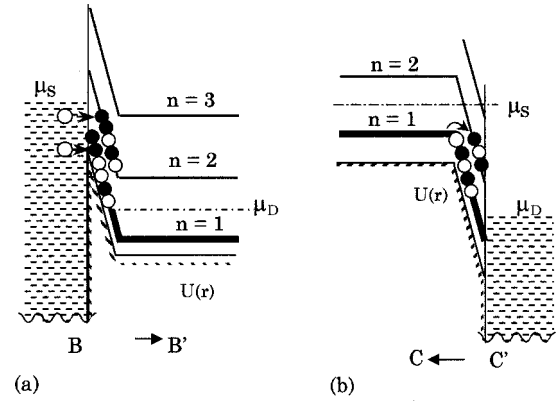


FIG. 9. Schematic representations of Landau levels together with the electrostatic potential $U(r)$; (a) in the vicinity of the lower corner $B$ of the $\mu_S$ contact along the cross section $B$-$B'$ in Fig. 7(c) and (b) in the vicinity of the lower corner $C'$ of the $\mu_S$ contact along the cross section $C$-$C'$ in Fig. 7(c).

that it leads to generation of nonequilibrium electron distribution on the 2DEG side without yielding finite $R_{xx}$, $R_{SC}$, or $R_{DC}$, as we will discuss below. Figure 9(a) schematically shows Landau levels together with the electrostatic potential $U(r)$ in the vicinity of the lower corner $B$ of the $\mu_S$ contact along the cross section $B$-$B'$ in Fig. 7(c). Here, electrons are injected into the 2DEG only via tunneling. Because the tunneling probability cannot be unity the highest occupied Landau level ($n = 1$ level in the figure) is not completely filled with electrons, being left with certain unoccupied states (holes). At the same time, electrons will be injected through tunneling to still higher Landau levels as illustrated in Fig. 9(a). Thus local nonequilibrium electrons (holes) are introduced in the vicinity of this corner, and will release their excess energies via emissions of phonons and partly via CE; viz, $P_{S-2\text{DEG}} > 0$. Thus the experimental finding that CE appears when $V_{SD} = \Delta\mu_{SD}/e > \hbar\omega_c/2e$ is explained.[27]

Figure 9(b) schematically shows Landau levels along the cross section $C$-$C'$ in Fig. 7(b) near the upper corner $C'$ of the drain contact. The physical situation at this electron exit corner is different from that of the electron entry corner because the exit of electrons to the drain contact is not disturbed by any potential barrier. It is important, however, that the higher empty Landau levels come close to the completely occupied Landau level ($n = 1$) due to the gradient of the potential fall. It follows that electrons will tunnel from the occupied Landau level ($n = 1$) to the higher empty Landau levels leaving holes in the lower level ($n = 1$) and creating excited electrons in the higher levels ($n > 1$). Thus local nonequilibrium distribution is expected to occur also in the vicinity of this electron exit corner; viz, $P_{D-2\text{DEG}} > 0$.[28] The experimentally observed CE at the drain-side corner is thus explained.

Based on this model, and following the scheme described in Ref. 4, we can derive $P_{S-2\text{DEG}} = (\nu/2h)\{\Delta\mu_{SD}^2 - (\hbar\omega_c/2)^2\}$ and $P_{D-2\text{DEG}} = (\nu/2h)(\Delta\mu_{SD} - \hbar\omega_c/2)^2$, respectively, for the amplitude of dissipation at the electron entry and exit corners for $\Delta\mu_S \gg \hbar\omega_c/2$. Note that for $\Delta\mu_{SD} \gg \hbar\omega_c/2$ the sum $P_{S-2\text{DEG}} + P_{D-2\text{DEG}}$ nearly amounts to the total power, $(\nu/h)\Delta\mu_{SD}^2 = V_{SD}I = R_H I^2$, and $P_{S-2\text{DEG}}$ and $P_{D-2\text{DEG}}$ are nearly equal to each other. The former is in

accordance with the experimental fact that the energy conversion efficiency of the CE for the $R_H I^2$ term is on the same order as that for the $R_{xx} I^2$ term at $I = 50\,\mu$A. The latter may account for the experimental finding that the intensities of the CE from the electron entry and exit corners are comparable to each other for $I = 73\,\mu$A [Fig. 6(b)].

Finally, let us consider why the two-terminal resistance can remain quantized despite the substantial dissipation in the 2DEG. First, on the side of the source contact, if the region of nonequilibrium distribution of electrons would extend to reach the upper corner of the contact [Fig. 8(c)], the electrons in the upper edge states would be involved in the equilibration. The electrochemical potential of the upper edge states would then be lowered below $\mu_S$, yielding a finite $R_{xx}$ or $R_{SC}$. Our experiments (Fig. 6), however, show that the region of CE does not reach the other corner of the $\mu_S$ contact. Therefore, it is highly probable that the electrons have been almost completely equilibrated at the upper corner of the $\mu_S$ contact [Fig. 8(c)]. Under this condition, no scattering takes place for the electrons in the upper edge states and the electrochemical potential $\mu_S$ of the upper edge states is kept unchanged. Therefore, the energy dissipation on the 2DEG side of the electron entry corner yields neither a finite $R_{xx}$ nor $R_{SC}$. Second, on the side of the drain contact, the region of inter-Landau-level tunneling will spread to a certain extent along the potential fall. However, this region is not expected to reach the lower corner of the drain contact at any occasion because the spatial separation caused by the fully occupied bulk states lying below $\mu_D$ will prevent the nonequilibrium electrons from being scattered to the lower edge states [Fig. 8(c)]: This is consistent with the observed profile of CE [Fig. 6(b)]. This implies that all the nonequilibrium electrons enter the $\mu_D$ contact without being backscattered and the electrochemical potential along the lower edge states is kept unchanged at $\mu_D$. Hence the energy dissipation on the 2DEG of the electron exit corner also yields neither finite $R_{xx}$ nor $R_{DC}$. The two-terminal resistance, $R_{st} = R_H + R_{xx} + R_{SC} + R_{DC}$, in the QHE state is thus quantized to $R_H$ despite the dissipation in the 2DEG at the current entry and exit corners.

### C. Cyclotron effective mass

The cyclotron effective mass $m_c^*$ derived from the observed cyclotron emission is $(0.069 \pm 0.0007)m_0$ both in the corners of the source and drain contacts. Additional experiments show that the $m_c^*$ does not change appreciably with $I$ in the range from $1\,\mu$A to $80\,\mu$A. The $m_c^*$ value brings information about an average energy of relevant nonequilibrium electrons because $m_c^*$ is affected by the conduction-band nonparabolicity.[29] In the present experiments with $\hbar\omega_c = 10$ meV, the expected $m_c^*$ values are such that $0.0690m_0$ ($n = 2 \rightarrow 1$), $0.0715m_0$ ($n = 3 \rightarrow 2$), and $0.0740m_0$ ($n = 4 \rightarrow 3$) for the respective Landau level transitions. The observed emission spectra are sharp enough [Fig. 2(c)] to resolve these transitions if they coexist, but we observe only one emission line corresponding to the transition $n = 2 \rightarrow 1$. This is consistent with our estimate of the effective electron temperature, $T_e \sim 10$ K. Nonequilibrium electrons must be excited in higher Landau levels of the indexes reaching $n = 60$–$100$ at $I = 50$–$80\,\mu$A. However, we suppose that these

energetic electrons are rapidly cooled down (to $T_e \sim 10$ K), before contributing to the CE, via the emission of optical phonons ($\hbar\omega_{opt} = 37$ meV) and the cyclotron phonon emission.[10]

## V. CONCLUSION

Experimental evidence has shown that CE occurs in QHE Hall bars ($B \sim 6$ T, $\nu = 2$) under the condition $R_{xx} + R_{SC} + R_{DC} \approx 0$ at $I = 10$–$80\,\mu$A. The effective electron temperature $T_e$ relevant to the CE for $I = 50$–$73\,\mu$A is roughly estimated to be 10 K. The CE is observed only in the range $V_{SD} > \hbar\omega_c/2e = 5$ mV ($I > 0.4\,\mu$A) but is not observed in the lower range $V_{SD} < \hbar\omega_c/2e$ ($I < 0.4\,\mu$A). This strongly suggests that for $V_{SD} < \hbar\omega_c/2e$ local nonequilibrium electron distribution is absent in the 2DEG and dissipations occur totally within the contacts; viz., $P_{S-2DEG} + P_{D-2DEG} = 0$ and that for $V_{SD} > \hbar\omega_c/2e$ nonequilibrium electron distribution is produced to cause dissipation in the 2DEG; viz., $P_{S-2DEG} + P_{D-2DEG} > 0$. Spatially resolved measurements at $I = 73\,\mu$A have revealed that the CE with comparable intensities occurs at both the current entry and exit corners, suggesting that $P_{S-2DEG} \sim P_{D-2DEG}$ at $I = 73\,\mu$A. The cyclotron effective mass, $m_c^* = (0.069 \pm 0.0007)m_0$, determined from the CE spectra for $1\,\mu$A $< I < 80\,\mu$A, indicates that only the lowest excited Landau level is relevant to the CE ($n = 2 \rightarrow 1$). This is consistent with the estimation of $T_e \sim 10$ K.

It is suggested that the QHE-breakdown-induced electron heating at the corners of a Hall conductor is not an appropriate explanation of the CE observed in the present experiments. We have proposed a theoretical model of current contacts and discussed in detail electron kinetics at the current entry and exit corners. This model suggests that a finite $V_{SD}$ intrinsically leads to formation of a potential barrier and a potential fall, respectively, at the electron entry and exit corners. For $V_{SD} < \hbar\omega_c/2e$, only edge states are relevant to the conduction.[26] The entry (exit) of electrons into (out of) the edge states is not disturbed by the potential barrier or fall. Accordingly local nonequilibrium distribution is absent in the 2DEG and all dissipations occur within the contacts; viz., $P_{S-2DEG} + P_{D-2DEG} = 0$. For $V_{SD} > \hbar\omega_c/2e$, not only edge states but also bulk states in the interior region contribute to the conduction. The entry (exit) of electrons into (out of) the bulk states is affected by the potential barrier and fall, leading to generation of nonequilibrium electron distribution on the 2DEG side of the respective corners. Thus dissipation occurs in the 2DEG: viz., $P_{S-2DEG} + P_{D-2DEG} > 0$ for $V_{SD} > \hbar\omega_c/2e$. It is suggested also that the fraction of dissipation on the 2DEG side increases to cover nearly the total power dissipation, $P_{S-2DEG} + P_{D-2DEG} \sim R_H I^2$, and the dissipation is nearly symmetric between the two corners, $P_{S-2DEG} \sim P_{D-2DEG}$, for $V_{SD} \gg \hbar\omega_C/2$. All these predictions are in good agreement with the experimental findings summarized in the above.

The vanishing of $R_{xx} + R_{SC} + R_{DC}$, or the quantization of $R_{2t}$, is suggested in the model to be equivalent to the requirement that the regions of the nonequilibrium distribution, primarily created at the electron entry and exit corners, do not extend over the full width of the boundary between the 2DEG and the contacts. The profile of the CE studied at $I = 73\,\mu$A indicates that this condition is satisfied, being con-

sistent with the experimentally confirmed absence of $R_{xx}$, $R_{SC}$, and $R_{DC}$.

All the experimental results have thus been reasonably interpreted in terms of a consistent picture of the electron kinetics at the current entry and exit corners of a QHE Hall bar.

*Present address: NEC Optoelectronics and High Frequency Device Research Laboratories, Miyukigaoka 34, Tukuba-shi, Ibaraki 305-8501, Japan.

[1] K. von Klitzing, G. Dorda, and M. Pepper, Phys. Rev. Lett. **45**, 494 (1980).

[2] S. Kawaji and J. Wakabayashi, in *Physics in High Magnetic Fields*, edited by S. Chikazumi and N. Miura (Springer, Berlin, 1981), p. 284.

[3] M. Büttiker, Phys. Rev. B **38**, 9375 (1988).

[4] S. Komiyama and H. Hirai, Phys. Rev. B **40**, 7767 (1989).

[5] U. Klaß, W. Dietsche, K. von Klitzing, and K. Ploog, Z. Phys. B **82**, 351 (1991).

[6] J. Wakabayashi and S. Kawaji, J. Phys. Soc. Jpn. **44**, 1839 (1978).

[7] P. A. Russell, F. F. Ouali, N. P. Hewett, and L. J. Challis, Surf. Sci. **229**, 54 (1990).

[8] K. von Klitzing *et al.*, in *Proceedings of the 17th International Conference on the Physics of Semiconductors*, edited by J. D. Chadi and W. A. Harrison (Springer, New York, 1985), p. 271.

[9] N. N. Zinov'ev *et al.*, Semicond. Sci. Technol. **9**, 831 (1994).

[10] S. Roshko, W. Dietsche, and L. J. Challis, Phys. Rev. Lett. **80**, 3835 (1998).

[11] P. C. van Son and T. M. Klapwijk, Europhys. Lett. **12**, 429 (1990).

[12] P. C. van Son, G. H. Kruithof, and T. M. Klapwijk, Phys. Rev. B **42**, 11 267 (1990).

[13] S. Komiyama, Y. Kawano, and Y. Hisanaga, in *Proceedings of the 21st International Conference on Infrared and Millimeter Waves*, edited by M. von Ortenberg and H.-U. Mueller (Humboldt-Universität zu Berlin, Berlin, 1996), p. BT2; S. Komiyama *et al.*, in *Proceedings of the 6th International Symposium Nanostructures: Physics and Technology*, edited by Zh. Alferov and L. Esaki (Ioffe Institute, St. Petersburg, 1998), p. 140.

[14] K. Hirakawa *et al.*, in *Proceedings of the 23rd International Conference on the Physics of Semiconductors*, edited by M. Scheffler and R. Zimmermann (World Scientific, Berlin, 1996), p. 2543.

[15] See, for example, F. Thiele *et al.*, Solid State Commun. **62**, 841 (1987).

[16] G. Ebert *et al.*, J. Phys. C **16**, 5441 (1983).

[17] S. Komiyama *et al.*, Solid State Commun. **54**, 479 (1985).

[18] Y. Kawaguchi *et al.*, Physica B **227**, 183 (1996); Jpn. J. Appl. Phys., Part 1 **34**, 4309 (1995).

[19] S. Komiyama *et al.*, Phys. Rev. Lett. **77**, 558 (1996).

[20] D. C. Tsui, G. J. Dolan, and A. C. Gossard, Bull. Am. Phys. Soc. **28**, 365 (1983).

[21] L. Eaves and F. W. Sheard, Semicond. Sci. Technol. **1**, 356 (1986).

[22] K. Yoshihiro *et al.*, Surf. Sci. **170**, 193 (1986).

[23] H. Hirai and S. Komiyama, Phys. Rev. B **49**, 14 012 (1994).

[24] S. Kawaji, in *Proceedings of the International Symposium on Foundations of Quantum Mechanics in the Light of New Technology*, edited by S. Kamefuchi *et al.* (Physical Society of Japan, Tokyo, 1984), p. 327.

[25] S. Komiyama and H. Hirai, Phys. Rev. B **54**, 2067 (1996); H. Hirai and S. Komiyama, Jpn. J. Appl. Phys., Part 1 **34**, 4321 (1995).

[26] This statement does not imply that the ''local current distribution'' is finite only at the edge states for $\Delta\mu_{SD} < \hbar\omega_c/2$. The ''local current distribution'' usually refers to the local change of the current density from the equilibrium state (Ref. 25), which in the present model is uniformly distributed over the full width of the conductor.

[27] At absolute zero temperature and without electron-electron scattering, no electrons (holes) would be excited above $\mu_S$ (below $\mu_D$), so that $\Delta\mu_{SD} = \hbar\omega_c$ would be predicted for the threshold value of the CE. In reality, however, electrons (holes) can be excited beyond $\mu_S$ (below $\mu_D$) via the electron-electron scattering once nonequilibrium electrons are introduced. The CE is therefore expected to occur for $\Delta\mu_{SD} > \hbar\omega_c/2$.

[28] It is possible that the threshold $\Delta\mu_{SD}$ value for $P_{D-2DEG}$ is somewhat larger than $\hbar\omega_c/2$ because higher local electric fields may be required for the Zener-type tunneling processes to occur. However, this does not substantially alter the discussion of this work.

[29] W. Zawadzki, C. Chaubet, D. Dur, W. Knap, and A. Raymond, Semicond. Sci. Technol. **9**, 320 (1994).